Segregation of O2 and CO on the surface of dust grains determines the desorption energy of O2

J. Noble, S. Diana, F. Dulieu

▶ To cite this version:

HAL Id: hal-01948057
https://hal.science/hal-01948057

Submitted on 11 Jan 2019

Segregation of O$_2$ and CO on the surface of dust grains determines the desorption energy of O$_2$

J. A. Noble,[★] S. Diana and F. Dulieu[†]

[1]*LERMA, Université de Cergy Pontoise, 5 mail Gay Lussac, F-95000 Cergy Pontoise Cedex, France*
[2]*LERMA, Observatoire de Paris, PSL Research University, CNRS, UMR 8112, Sorbonne Universités, UPMC Univ Paris 06, Paris, France*

ABSTRACT

Selective depletion towards pre-stellar cores is still not understood. The exchange between the solid and gas phases is central to this mystery. The aim of this paper is to show that the thermal desorption of O$_2$ and CO from a submonolayer mixture is greatly affected by the composition of the initial surface population. We have performed thermally programmed desorption (TPD) experiments on various submonolayer mixtures of O$_2$ and CO. Pure O$_2$ and CO exhibit almost the same desorption behaviour, but their desorption differs strongly when mixed. Pure O$_2$ is slightly less volatile than CO, while in mixtures, O$_2$ desorbs earlier than CO. We analyse our data using a desorption law linking competition for binding sites with desorption, based on the assumption that the binding energy distribution of both molecules is the same. We apply Fermi–Dirac statistics in order to calculate the adsorption site population distribution, and derive the desorbing fluxes. Despite its simplicity, the model reproduces the observed desorption profiles, indicating that competition for adsorption sites is the reason for lower temperature O$_2$ desorption. CO molecules push-out or 'dislodge' O$_2$ molecules from the most favourable binding sites, ultimately forcing their early desorption. It is crucial to consider the surface coverage of dust grains in any description of desorption. Competition for access to binding sites results in some important discrepancies between similar kinds of molecules, such as CO and O$_2$. This is an important phenomenon to be investigated in order to develop a better understanding of the apparently selective depletion observed in dark molecular clouds.

Key words: astrochemistry – molecular data – molecular processes – methods: laboratory: molecular – ISM: molecules.

1 INTRODUCTION

Star formation occurs in the dense cores of very cold interstellar clouds, where most volatile species disappear from the gas phase early in the process (Bergin & Tafalla 2007). The molecules stick to the surface of dust grains, forming icy mantles. Some species, such as CO, exhibit heavy depletion, or 'freeze-out', in molecular cores (Caselli et al. 1999; Bacmann et al. 2002; Pagani, Bourgoin & Lique 2012), while other dust tracers, like N$_2$H$^+$, remain abundant in the same regions (Pagani et al. 2007). Certain species which, according to theoretical predictions, should be present in the gas phase, like O$_2$, are not detected, while others, such as CH$_3$OCH$_3$, seem to be present in excess (Bacmann et al. 2012). Yet others, among them H$_2$O, are detected in excited states, the reasons for which are not yet clear (Lis et al. 2013). Overall, the freeze-out process is far from being understood. An indirect consequence of the freeze-out mechanism is its possible role in the triggering of the final collapse phase, required to form and ignite the new star, and thus a better understanding of these mechanisms would also help to constrain the age of pre-stellar cores (Honvault et al. 2011).

Although models predict that accretion should lead to all molecules being frozen on to grains on the time-scale of core formation, various desorption processes are also active in star forming regions (Willacy & Millar 1998). In addition to thermal desorption (e.g. Burke & Brown 2010), other mechanisms such as photodesorption (e.g. Öberg, van Dishoeck & Linnartz 2009; Bertin et al. 2013) or chemical desorption (Dulieu et al. 2013) return molecules to the gas phase despite the low temperature. The current description of desorption does not, in itself, explain why, for example, two molecules with identical masses, similar sticking

[★]Present address: Université de Bordeaux, Institut des Sciences Moléculaires UMR 5255 CNRS, 351 cours de la Libération, F-33405 Talence, France.
[†]E-mail: francois.dulieu@obspm.fr

coefficients, and comparable multilayer binding energies (Bisschop et al. 2006), CO and N$_2$, exhibit fundamentally different depletion behaviour, with N$_2$ observed in the gas phase after depletion of CO (Pagani et al. 2012). Nor does it explain the non-detection of gas phase O$_2$, except for three low abundance observations: an upper limit ($<5 \times 10^{-8}$/H$_2$) towards the cloud core ρ Oph A (Larsson et al. 2007), in emission ($\sim 4 \times 10^{-6}$/H$_2$) towards Orion KL (Goldsmith et al. 2011), and, most recently, an upper limit ($\leq 6 \times 10^{-9}$/H$_2$) towards the deeply embedded low-mass Class 0 protostar NGC 1333-IRAS 4A (Yıldız et al. 2013). One explanation is that grain surface chemistry plays an important role in transforming adsorbed molecules, removing small molecules from the adsorption–desorption cycle by the formation of more complex species (e.g. Hama & Watanabe 2013). Another may be that the fundamental processes of adsorption and desorption, governed by the binding energies of molecules to the bare grain surface or the icy mantle, have yet to be fully understood. In particular, the roles of submonolayer coverages and molecular mixtures have not yet been defined.

Acharyya et al. (2007) showed that, in the multilayer regime, O$_2$ and CO molecular ices have similar binding energies. O$_2$ is slightly less volatile than CO, with a binding energy of 912 ± 15 versus 858 ± 15 K for pure ices. A recent study by Collings et al. (2015) found comparable values of 902 ± 24 and 878 ± 36 K, respectively. In the multilayer regime, the mixing of these ices slightly affects the desorption experiments but seems to have no important consequences in an astrophysical context (Acharyya et al. 2007). However, we have previously demonstrated (Noble et al. 2012) the dependence of the binding energy of these species on the nature of the underlying substrate and, more importantly, the coverage, for desorption occurring in the submonolayer regime. For example, on a non-porous amorphous solid water (np-ASW) surface, the effective binding energy of a full monolayer (ML) of CO is 863 K (i.e. equivalent to the multilayer energy; e.g. Acharyya et al. 2007), while at a coverage of 0.1 ML, the effective binding energy is 1307 K, an increase of $\sim$ 50 per cent (Noble et al. 2012). We showed that the effect is even more marked for an amorphous silicate substrate, where the CO monolayer binding energy is 867 K and the effective binding energy at 0.1 ML is 1418 K. This coverage dependence was confirmed by Collings et al. (2015), who determined a desorption energy of 1191–1407 K for 0.06 ML of CO desorbing from an amorphous silica substrate (compared to 878 K for the full monolayer/multilayer).

No studies have yet been performed to investigate the effect of ice mixtures on the desorption characteristics of the species in submonolayer conditions, i.e. relevant to low coverages on interstellar dust grains.

For the CO molecule, existing largely in the solid state in cloud cores (Tielens et al. 1991; Whittet & Duley 1991; Chiar et al. 1995; Pontoppidan et al. 2003), this huge observed variation in the binding energy will have a dramatic effect on its desorption flux.

Using the standard Polanyi–Wigner equation, the desorption flux can be calculated as follows:

$$\phi_{\text{out}} = AN^n e^{-E_{\text{b}}/k_{\text{b}}T_{\text{s}}}, \tag{1}$$

where ϕ_{out} is the desorbing flux (ML s^{-1}), A is the pre-exponential factor, N is the number of adsorbed molecules on the surface (cm^{-2}), n is the order of the reaction, E_{b} is the binding energy (eV), k_{b} is the Boltzmann constant (eV molecules^{-1} K^{-1}), and T_{s} is the temperature of the surface (K). The units of A depend on n: molecules^{1-n} cm^{-2+2n} s^{-1}.

Multilayer desorption typically exhibits zeroth-order kinetics, and the equation simplifies to

$$\phi_{\text{out}}^{\text{mult}} = A e^{-E_{\text{b}}^{\text{mult}}/k_{\text{b}}T_{\text{s}}}, \tag{2}$$

while (sub)monolayer desorption typically exhibits first-order kinetics, and can be described as

$$\phi_{\text{out}}^{\text{sub}} = AN e^{-E_{\text{b}}^{\text{sub}}/k_{\text{b}}T_{\text{s}}}. \tag{3}$$

We make the standard assumptions that one monolayer is composed of 10^{15} molecules cm^{-2}, the density of sites on the surface of compact ice, and that the pre-exponential factor, A, can be fixed at $A = 10^{12}$.

For any number of adsorbed molecules, N, we can calculate the ratio of the desorbing fluxes in the multilayer regime (1 ML) and the submonolayer regime (0.1 ML) by

$$\frac{\phi_{\text{out}}^{\text{mult}}}{\phi_{\text{out}}^{\text{sub}}} = \exp[(E_{\text{b}}^{\text{sub}} - E_{\text{b}}^{\text{mult}})/k_{\text{b}}T_{\text{s}}]. \tag{4}$$

At 10 K, this ratio corresponds to a difference of 19 orders of magnitude in the desorbing fluxes, demonstrating that we must confront the question of coverage-dependent desorption in interstellar environments. However, at 10 K, it is also true that both desorbing fluxes are so low that thermal desorption cannot be considered as a realistic mechanism to replenish the gas phase. When the temperature rises to 20 K, the ratio is still large (9 orders of magnitude) and the desorption flux is now relevant to interstellar conditions.

In the laboratory, binding energies are derived from thermally programmed desorption (TPD) spectra such as those shown in Fig. 1, adapted from Noble et al. (2012). In this example, various (known) doses of CO (upper panel) or O$_2$ (lower panel) are deposited on np-ASW. The experimental TPD profiles (traced with crosses), which measure the desorption process, exhibit a filling behaviour, described in detail in Kimmel et al. (2001). To summarize, at a low coverage (small dose), molecules occupy the most energetically favourable adsorption sites and are tightly bound to the surface, desorbing late in the TPD at high temperatures (in this case, between $\sim$40 and 50 K). As the surface coverage increases, molecules are forced to populate progressively less tightly bound sites, provoking earlier desorption. This progressive adsorption behaviour continues until the first surface layer is complete, at a coverage of 1 ML. Thus, the leading edge of the spectra varies greatly with the dose and carries information about the surface coverage. When the leading edge no longer shifts towards lower temperatures, this indicates that a full monolayer has been deposited. One notable feature of the submonolayer filling behaviour is that, for a family of TPD spectra of varying coverages, a common tail is observed at high temperatures. It is this tail which is key to estimating the binding energy distribution across the various surface binding sites.

At higher (i.e. multilayer) coverages, the O$_2$–O$_2$ interaction becomes stronger than the surface–O$_2$ interaction, and the leading edge of the TPD spectra begins to shift back to higher temperatures, with the species exhibiting so-called zeroth-order desorption behaviour. Simulated zeroth-order desorption kinetics for both CO and O$_2$ are traced in black on Fig. 1, using the energies derived by Acharyya et al. (2007). Similarly, first-order desorption spectra are derived for each experimental surface coverage (traced in solid coloured lines). This figure illustrates the risk of applying multilayer desorption energies to the kinetics of submonolayer desorption (a traditional approach in gas–grain models). The simulated TPD spectra reproduce the desorption of the first few molecules at $\sim$25 K relatively well, but rapidly deviate from the experimental data at higher temperature, particularly in the case of CO. The simulated
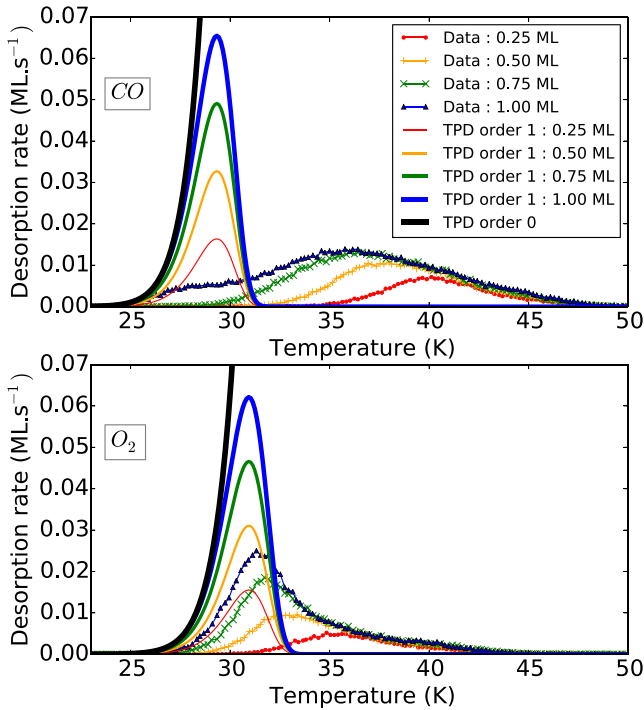
Figure 1. Pure CO (top) and O_2 (bottom) desorption profiles of approximately 0.25 (red), 0.5 (yellow), 0.75 (green), and 1 (blue) ML of adsorbate from non-porous amorphous water ice (data from Noble et al. 2012). Experimental data are represented with crosses. Black solid lines represent the simulated zeroth-order multilayer desorption kinetics, and coloured solid lines correspond to first-order desorption, simulated using a constant binding energy (E_b(CO) = 912 K, E_b(O_2) = 858 K; Acharyya et al. 2007), as is usual in astrophysical models.

spectra rely on describing a complex desorption phenomenon with a single binding energy, while the (real) measured desorption has a wide distribution of binding energies. It is important to develop a simple mathematical description of this energy distribution that can be integrated into astrochemical gas–grain models, and such a method has been developed by Amiaud et al. (2015).

It is clear that the coverage of the adsorbed species can greatly influence the desorption although, of course, there are further physical and chemical processes which are linked to gas phase abundance variations. One important variable to consider is the grain surface chemistry, dominated by diffusion of reactants. In many astrochemical models treating grain surface chemistry, the diffusion energy is assumed to be a constant fraction (between 0.3 and 0.7) of the multilayer desorption energy. Therefore, changing the desorption properties changes the diffusion properties, and thus the chemistry. In our recent studies of H_2O and CO_2 formation (Dulieu et al. 2010, 2013; Noble et al. 2011; Chaabouni et al. 2012; Minissale et al. 2013; Minissale, Congiu & Dulieu 2014), we have clearly demonstrated that CO and O_2 are important precursors to these two ubiquitous components of interstellar ices. Now that the key chemical role of these small molecules is understood, it is necessary to revisit their thermal desorption characteristics in the submonolayer regime and, importantly, in mixtures relevant to ice mantles on grain surfaces.

The major aim of this article is to unveil the importance of mixtures of surface adsorbates to the desorption characteristics of each molecular species. In Section 2, we will show that, unlike in the multilayer regime (Acharyya et al. 2007), the submonolayer desorption

Table 1. Values of the deposited dose of O_2 and CO on np-ASW. One set is in the submonolayer regime ('sub'), and second set corresponds to the beginning of multilayer regime (the total coverage of both deposited species is greater than 1 ML, 'multi').

Type	Sub	Sub	Sub	Sub	Sub	Sub	Sub
O_2	0.4	0.1	0.4	0.7	0.1	0.2	0.3
CO	0.5	0.7	0.4	0.1	0.3	0.2	0.1
Type	Multi	Multi	Multi	Multi	Multi	Multi	–
O_2	0.8	0.5	0.4	0.3	0.7	0.7	–
CO	1.0	0.6	0.7	0.8	0.6	1.0	–

behaviour of O_2 and CO mixtures is strikingly different to the desorption of each individual species. In submonolayer mixtures, O_2 desorption occurs at lower temperatures due to the presence of CO, whereas CO desorption remains effectively unchanged. In Section 4, we will apply a surface segregation model, developed by Amiaud et al. (2015), to experimental TPD spectra of mixtures of CO and O_2. The model is able to reproduce the desorption behaviour of both adsorbates using a simple Fermi–Dirac statistical approach. In order for our results to be more easily implemented into astrochemical models, we also derive effective desorption energies as a function of initial O_2 and CO coverages for various mixtures. In Section 5, we will discuss how these findings change our vision of the adsorption–desorption process, and show that the range of dust temperatures where segregation on the grain surface will play a critical role is rather wide (15–25 K).

2 EXPERIMENTS

All experiments were performed using the FORMOLISM set-up (e.g. Congiu et al. 2012). A non-porous, compact ASW ice sample (~ 50 ML) is grown by gas phase deposition on to a gold mirror held at 110 K. We deposit molecules on the ASW sample held at 18 K using one triply pumped molecular beam of, alternately, O_2 or CO (at a flux of about 3×10^{12} mol cm^{-2} s^{-1}). After deposition of both molecules (for varying times, see below), the sample temperature is ramped linearly at 10 K min^{-1}. Both molecular signals (*m/z* 32 and 28) are simultaneously monitored upon desorption by a Quadripole mass spectrometer (QMS) positioned directly in front of the surface. Thanks to the use of the molecular beam, there is almost no parasitic desorption from other parts of the cooling system, except a tiny, constant signal which is subtracted. The coverage of each molecule is calibrated by searching for the multilayer feature (see Noble et al. 2012). CO and O_2 are alternated in the beam without any visible effect on the curves. Thus, although a small pollution (<5 per cent) of one molecular species could be present in the beam of the other species, it does not affect the results at all, since (i) the real initial coverage is calculated precisely after desorption, and (ii) both molecules are well separated by the QMS. Table 1 details all the experiments performed, which fell into one of two categories: the 'sub' experiments correspond to the situation where the total coverage of adsorbed molecules is kept below the monolayer, while the 'multi' experiments fill the gap between our 'sub' experiments and the multilayer conditions already described by Acharyya et al. (2007).

3 EXPERIMENTAL RESULTS

Fig. 2 shows TPD spectra of an intermediate 'multi' case with a total deposition coverage lower than the previously studied multilayer
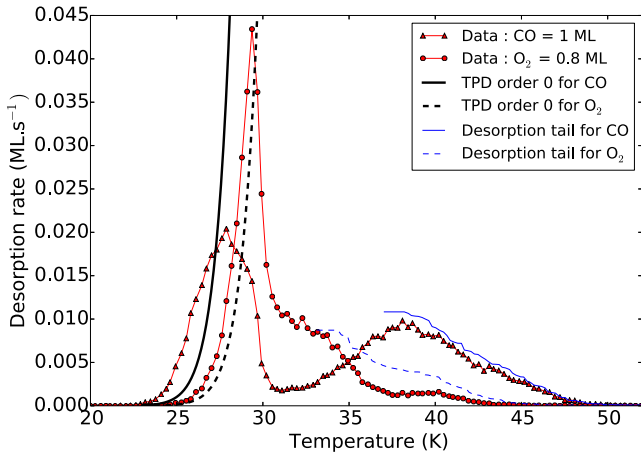
Figure 2. TPD profiles of 1.0 ML of CO (red solid line) and 0.8 ML of O$_2$ (red dashed line) desorbing from np-ASW ice. Calculated leading edges (black) of CO and O$_2$, representing the multilayer regime, and desorption tails (blue), representing the submonolayer regime of pure gas, are also represented.
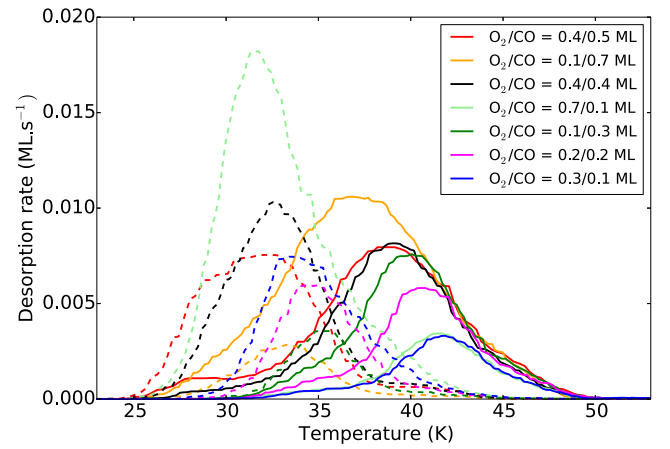

Figure 3. Submonolayer regime TPD profiles of various mixtures of CO and O$_2$ deposited on a np-ASW substrate. Each colour corresponds to one experiment. CO and O$_2$ spectra are plotted with solid and dashed lines, respectively.
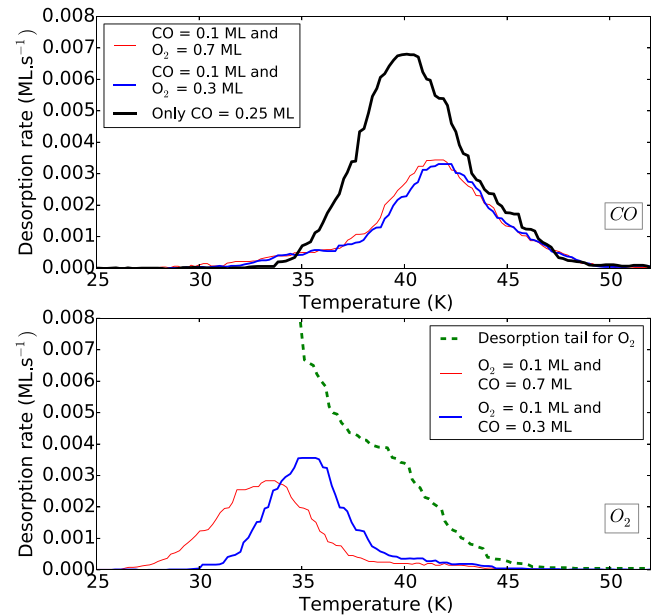

Figure 4. Upper panel: 0.1 ML of CO desorbing from np-ASW, in mixtures with 0.3 (blue), and 0.7 ML (red) of O$_2$. Also shown is the desorption of 0.25 ML of pure CO (black). Lower panel: 0.1 ML of O$_2$ desorbing from np-ASW, in mixtures with 0.3 (blue), and 0.7 ML (red) of CO. Also shown is the desorption tail of the pure O$_2$ monolayer.

regime (Acharyya et al. 2007) but higher than the submonolayer regime in our new 'sub' study. The total coverage is 1.8 ML (1.0 ML CO plus 0.8 ML O$_2$). At low temperatures, we see that both CO and O$_2$ have reached the multilayer leading edge. Furthermore, we see that CO desorbs first, with O$_2$ desorbing at higher temperature, confirming the finding of Acharyya et al. (2007) that CO is more volatile than O$_2$ in the case of multilayer mixtures. The match of the leading edge is not perfect, however, because with a total of 1.8 ML, the substrate probably still affects the desorption. Also, in the case of CO, the multilayer regime is known to appear more clearly above a few multilayers, as can be seen in fig. 1 (upper middle panel, inset) of Noble et al. (2012). At the highest desorption temperatures, in the submonolayer regime, we can see two different desorption behaviours. CO desorbs following its regular desorption tail, indicating that it is not perturbed by the presence of O$_2$, but O$_2$ does not follow its normal desorption tail, desorbing earlier than in the case of pure O$_2$.

In all other multilayer experiments detailed in Table 1, O$_2$ is pushed towards its multilayer leading edge, desorbing before the normal desorption tail of pure O$_2$, whereas CO follows its regular desorption tail (between ∼37 and 50 K), confirming its filling behaviour. The O$_2$ profiles are restricted to the intermediate 25–35 K temperature window, while CO is quenched in the 37–50 K region.

For the rest of this article, we will focus on the submonolayer subset of experiments. Fig. 3 shows the desorption of various submonolayer mixtures of O$_2$ (dashed lines) and CO (solid lines). Each colour corresponds to one experiment, and in each experiment the total surface coverage was kept below the monolayer. The first important point to note is that, when we consider the whole subset of submonolayer desorption experiments, we observe an inversion in the desorption order of O$_2$ and CO compared to the multilayer. In the multilayer regime, CO desorbs first, whereas in the submonolayer regime, O$_2$ desorbs first. We can also observe that, for CO, the common tail above 40 K is present, almost unperturbed compared to pure CO desorption experiments (Fig. 1). This means that CO follows a filling behaviour desorption and seems to be unaffected by the presence of O$_2$. On the other hand, the tails of the O$_2$ spectra are rather dispersed, and the various spectra no longer share the common tail observed in Fig. 1, where no CO was perturbing the O$_2$ desorption. The global trend is that the O$_2$ molecules seems to

desorb earlier, and before the CO molecules. More specifically, it appears that the more CO is co-adsorbed on the surface, the earlier the O$_2$ molecules desorb from the surface.

The segregation of O$_2$ and CO in the submonolayer regime is highlighted by the examples given in Fig. 4. In the upper panel of Fig. 4, we see that 0.1 ML of CO follows its 'pure' desorption tail when mixed with 0.3 and 0.7 ML of O$_2$, almost unperturbed by the relatively large amount of O$_2$ co-adsorbed on the surface. The lower panel of Fig. 4, however, illustrates explicitly the behaviour of about 0.1 ML of O$_2$ in different environments. The dashed green line shows the normal desorption tail for pure O$_2$, the blue line is O$_2$ co-adsorbed with 0.3 ML of CO, and the red line is O$_2$ co-adsorbed with 0.7 ML of CO. We can see a dramatic shift of the desorption

towards colder temperatures with the addition of CO. Moreover, the O_2 traces are clearly not following the 'pure' desorption tail.

O_2 molecules are clearly pushed to less favourable surface adsorption sites by the presence of CO molecules, ultimately resulting in the earlier desorption of O_2 during heating. It is important to note that the molecules of the two species rearrange their positions on the surface, but none are directly ejected into the gas phase during the process. This 'dislodging' mechanism, where molecules of one chemical species deplace another on the surface, has been already encountered in the case of D_2 and H_2 mixtures (Dulieu et al. 2005), and has been discussed in an astrophysical context by Kristensen et al. (2011). A desorption model was developed in these studies, capable of reproducing the distortion in the TPD spectra of mixtures. It was even applied to the desorption of ortho and para D_2 from porous water (Amiaud et al. 2008), allowing the measurement of a tiny (1.4 meV) difference in the binding energy of the two states. In the present study, we will apply basically the same model to the submonolayer data presented above.

4 DESORPTION MODELLING INCLUDING SURFACE SEGREGATION MECHANISMS

Most models used to reproduce desorption of lab data only deal with a single molecular species. Sometimes, models consider different molecules to behave differently (e.g. Fayolle et al. 2011) or are focused on phenomena such as the reconstruction of the water ice network and trapping (e.g. Bossa et al. 2014).

For our experiments we need a model that includes both (i) a binding energy distribution, but also (ii) a redistribution factor for the two molecules, since they obviously behave differently. Here, we assume that the substrate is unchanged during the desorption and is comprised of adsorption sites equally attainable for all of the molecules. Both molecular species are in direct competition to populate the binding sites.

4.1 Binding energy distributions

We have previously described in detail the shape of the distribution of binding site energies, and it has been shown explicitly (see fig. 4 of Noble et al. 2012) that the distribution depends on both the type of surface and on the molecule desorbing from it. We can directly apply binding energy distributions derived in this manner to describe molecular desorption using an inverted Polanyi–Wigner equation (Dohnalek et al. (2001), the 'classical inversion method'). There are, however, certain assumptions behind the model used to determine these distributions, that make the distributions inappropriate for use in the current study. In particular, it is assumed that the binding energy (E_b) is only dependent on the coverage (θ). In the case where there are two kinds of molecules, the total coverage alone is not sufficient to describe the observed experimental trends. We cannot simply add CO and O_2, because CO and O_2 behave differently. Therefore, the binding energy distribution has to be derived from a law allowing both adsorbates to simultaneously populate their binding site distributions.

In our previous work on H_2 and its isotopes (Dulieu et al. 2005; Amiaud et al. 2006), we used the Fermi–Dirac statistical repartition law (see Section 4.2 for details) with great success. This approach is different from all other TPD analyses because the binding energy is not directly linked to the coverage. The molecules are distributed across all the different binding sites, but have a different probability of populating each site. Nevertheless, as for the filling behaviour description (described above), the most tightly bound sites will be the

most occupied at the low heating rates we use. As such, the classical inversion method used previously can be considered as an approximation of the distribution we would find when taking into account the Fermi–Dirac distribution. More precisely, the classical inversion method corresponds to the limit of the Fermi–Dirac distribution for a temperature of 0 K. In the classical inversion method, we consider that molecules do not spread over the distribution of sites, or, if they do so, we calculate an effective binding energy which is only dependent on the coverage, $E_b(\theta)$. Using the Fermi–Dirac distribution, we add a surface temperature dependence, $E_{bFD}(T_s, \theta)$, in order to calculate an effective energy. The use of the redistribution of molecules among the different binding sites is supported by the fact that, close to the desorption limit, diffusion is much faster than desorption. Usually, the diffusion, E_{diff}, is assumed to be a fraction, X, of the binding energy, E_b. Using two classical Arrhenius desorption and diffusion laws, we find that the ratio between diffusion and desorption rates is

$$\frac{r(\text{Diffusion})}{r(\text{Desorption})} = \exp\left(\frac{E_b - E_{diff}}{k_b T_s}\right) = \exp(1-X)E_b/k_b T_s. \quad (5)$$

To give an idea of the order of magnitude, we choose as an example $E_b = 1000$ K, $T_s = 30$ K, $X_{min} = 0.2$, and $X_{max} = 0.8$. In this case, the average number of diffusion hops before the desorption of a molecule is between approximately 10^3 and 10^{11}. Even though the diffusion is very limited, the number of diffusing events is certainly high before any desorbing event. Based on this observation, assuming a thermal equilibrium, as in the Fermi–Dirac distribution, sounds reasonable.

It is still necessary to determine the shapes which will be used to define the distributions. For H_2 and its isotopes, we successfully proposed that the binding energy distributions of each isotope have exactly the same shape, shifted in energy by a small amount due to the zero-point energy. For O_2 and CO, we cannot use the same zero-point energy argument. In the case of two different molecules the question becomes: are the most favourable adsorption sites the same for CO and for O_2? Here, we have indirect experimental evidence of the fact that it is the surface geometry that imposes the greatest variation in the binding energy. If CO and O_2 were not in competition for the same adsorption sites, but rather each adsorbate adsorbed preferentially to different geometric sites, there should be no (or less) competition. Thus, even though it is a large assumption, we adopt the same hypothesis for CO and O_2 as used previously for H_2 and its isotopes: the binding energy distributions of CO and O_2 are almost the same, except that there is a small, global shift in energy. This means that for each individual adsorption site, the binding energy of CO is slightly higher than that of O_2. We ground this hypothesis in the observation of the desorbing tails of CO and O_2, represented in blue in Fig. 2. They look roughly parallel, indicating that there is a global shift in energy.

For both CO and O_2, the binding energy distribution curves look very approximately like bells: a flat plateau on the maximum followed by a decreasing tail (see fig. 4 of Noble et al. 2012). To reproduce this shape, we tested first an asymmetric Gaussian distribution shape, finally choosing a symmetric Gaussian distribution due to satisfactory results in the model. The binding sites are described by a binding energy distribution, approximated here as a Gaussian function. Hereafter, we will use the simpler E instead of E_b to represent the binding energy.

$$g(E) = g_o \times \exp-\left(\frac{E_o - E}{\Delta E}\right)^2, \quad (6)$$

Table 2. Binding energy distribution of CO and O₂.

Molecules	E_o (K/k_b)	ΔE (K/k_b)
CO	1100	180
O₂	1015	180

where g_o is a normalizing coefficient ($\int_0^\infty g(E)dE = 1$), E_o represents the mean desorption energy, and ΔE the energy spread. $g(E)$ represents the number of sites between E and $E + dE$. The conditions of normalization correspond to a full occupation of binding sites (i.e. coverage equivalent to 1 ML).

We already know that this function will not perfectly reproduce all experimental features, since the real distribution shapes are not exactly Gaussian, and particularly since the optimum shapes are known to be different for each molecule. It is possible to find another, more precise, mathematical description of the binding sites, as we did previously (Noble et al. 2012), but here we only wanted to describe the trend in the effect of co-adsorption, our aim being to address the question of the competition for adsorption sites.

In summary, we propose that, due to the amorphous nature of the surface and the disorder in its topology, the binding energy of one adsorbate is not unique, but rather spread over a Gaussian distribution. The CO molecule is slightly more bound than O₂ (-180 K), but the energy dispersion is the same. The values are reported in Table 2. We assume that the topological disorder of the surface is the primary factor responsible for the binding energy spread. Over these two similar binding energy distributions, we must now distribute the populations of each molecule.

4.2 Distribution of molecules among the adsorption sites

Here, we assume that the adsorbate is spread over the binding sites following the Fermi–Dirac statistical equilibrium. For one adsorbate, this gives

$$p(E) = g(E) \left\{ 1 + \exp\left(\frac{E - \mu}{k_b T} \right) \right\}^{-1}, \qquad (7)$$

where $p(E)$ is the probability for the fraction of the distribution of sites between E and $E + dE$ to be populated. One can see that it depends on the chemical potential, μ, which in turn is linked to the total number of adsorbates, N. It can be computed at each step of the simulation by solving:

$$\int_0^\infty p(E)dE = N. \qquad (8)$$

Now we simply write the desorption probability. We integrate the desorption probability over the full binding energy distribution, weighted by the probability of occupying the given sites, as follows:

$$\phi_{out} = A \int_0^\infty p(E)e^{-E/k_b T} dE. \qquad (9)$$

Fig. 5 illustrates the binding energy distribution of CO (in blue), which resembles a Gaussian curve centred around 1100 K. We also include two distributions of 0.2 ML of molecules at $T = 10$ (black) and $T = 35$ K (red). We see that the molecules do not occupy the same sites at different temperatures. For the low temperatures, the distribution is almost entirely confined to the most bound sites, approximately down to 1200 K, whereas, for the 35 K distribution (which corresponds to the temperature where desorption starts to be measurable in the laboratory), some molecules occupy less tightly bound sites, down to 1000 K. This occupation, though transitional,
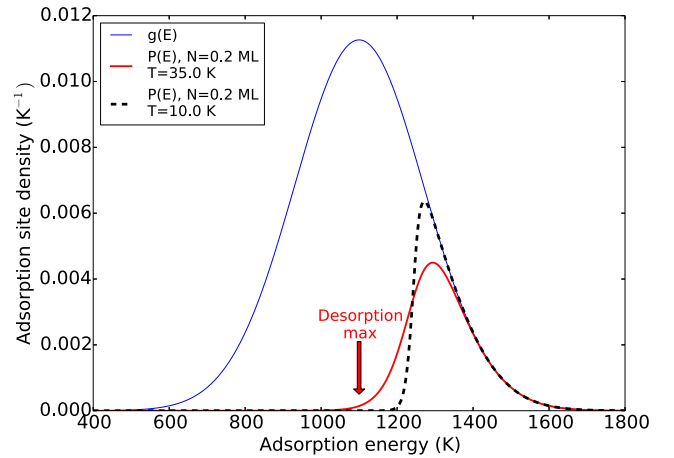

Figure 5. Total binding energy distribution of CO (blue), with distributions for 0.2 ML of CO at $T = 10$ (black) and $T = 35$ K (red). The red arrow indicates the energy of maximum desorption at $T = 35$ K.

is very important, because when we determine the sites from which the desorption originates, we observe that molecules mostly desorb from these less bound sites. On Fig. 5, a red arrow indicates the energy of the binding site from which the desorption contribution is maximal. It is close to 1100 K for this case. It is important to note that, even though the sites around 1100 K are not highly populated, they are the main sources of desorption.

Obviously this description of the desorption is much harder to simulate than the classical inversion method. The results provide a better match to the pure molecule experiments, especially on the leading edges of the spectra, but the extra cost seems unnecessary since the classical inversion method already gives a very satisfactory description of the desorption. However, using Fermi–Dirac statistics has the great advantage of providing a distribution of the adsorbates over the binding site distribution. It is therefore relatively easy to implement in the case of a mixture of adsorbates. We can rewrite equation (7) for CO, assuming that the number of sites available, $g(E)$, is reduced by the presence of the other adsorbate $p_{O_2}(E)$:

$$p_{CO}(E, T, \mu_{CO}, p_{O_2})$$
$$= (g_{CO}(E) - p_{O_2}(E)) \left\{ 1 + \exp\left(\frac{E - \mu_{CO}}{k_b T} \right) \right\}^{-1}. \qquad (10)$$

There is a similar equation for O₂ and there are two relationships required to calculate the two chemical potentials μ_{CO} and μ_{O2}. The coupled desorption of both adsorbates is calculated for each adsorbate, using equation (9), at each step of the simulation. More details about the model can be found in Kristensen et al. (2011) and Amiaud et al. (2015). The aim of this article is not to detail the specifics of the model, but rather to explain its utility in the case of mixtures.

To summarize, the use of a Fermi–Dirac thermal equilibrium relies on the hypothesis that the diffusion is sufficiently rapid to change the distribution of adsorbates during heating. This redistribution significantly influences the effective binding energy and it is why the binding energy distribution is slightly different than the one determined with the simpler classical inversion method, which is, itself, already a far better description of the desorption process than using a unique binding energy. The Fermi–Dirac analysis method is physically and computationally sophisticated, with the following intrinsic properties and advantages:
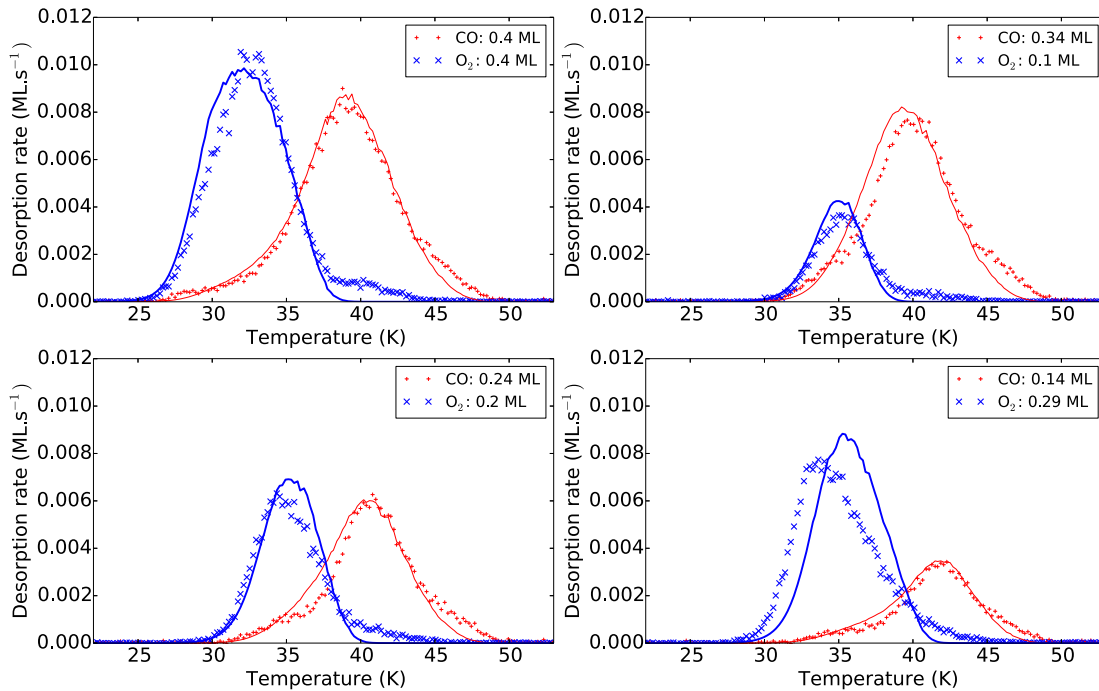
Figure 6. Four experimental and simulated TPD profiles of different mixtures of O_2 and CO deposited on np-ASW. Seven such experiments where the total coverage is less than 0.8 ML have been fitted simultaneously.

(i) The desorption occurs primarily from less energetically bound sites, despite the population of these sites being statistically low.

(ii) The use of the Fermi–Dirac statistical distribution on the binding sites tends to broaden the desorption profiles, in particular making the leading edge of the curves less steep, giving a better fit to the experimental data. Conversely, the classical inversion method provides a better fit to the desorbing tails and is less accurate in mimicking the leading edges.

(iii) As there is a unique distribution law, it is easy to consider different populations and to deal with their competition.

(iv) The assumption of a thermal equilibrium at experimental time-scales guarantees that there is no artefact when the results are transcribed to astrophysical time-scales.

4.3 Comparison between model and experiments

Fig. 6 shows four of the seven submonolayer CO:O_2 mixtures that have been fitted simultaneously. The solid lines represent the model whereas the crosses correspond to the experimental data. We have only adjusted the two E_o parameters (the median binding energy of each adsorbate) and used a common adjusted ΔE to ensure the minimum number of free parameters when testing the method. The results of the fitting procedure are very good. All the CO curves (in red) are nicely reproduced, and the O_2 desorption curves (in blue), although not perfectly reproduced, are very predictive. The case where the data are the least well fitted (bottom right panel) is where there is little CO (0.14 ML) and a larger dose of O_2 (0.29 ML). In the simulations, the desorption of O_2 happens a little late, therefore the binding energy distribution of O_2 is probably overestimated for low coverages. This is due to the choice of the shape of the distribution of binding energies, which is fitted principally to the CO distribution by the minimization procedure (a standard χ^2 method). It is clear that the CO curves are better fitted than the O_2; this is because the CO desorbs later and we know that the tail of the

desorption dominates the binding energy distribution. The O_2 distribution could be fitted separately, in order to increase the quality of the final fit, but we consider that it is not necessary to obtain the perfect experimental fit. We prioritize the development of a model based on simple assumptions, that will be easily applicable to grains in astrophysical conditions, where the exact composition of the surfaces is not well known and so neither are the exact binding energy distributions. The very good quality of the fit in Fig. 6 is the verification of our hypothesis that the competition for adsorption sites is the main physical source of the differentiated desorption of CO and O_2. Moreover, this behaviour can be modelled using Fermi–Dirac statistics applied to the distributions of adsorbate binding energies. The detail in the shape of the distribution does not play a very important role and, therefore, even if the surface is changed, the observed trend of the earlier desorption of O_2 should remain true.

4.4 Incorporation of the results into a traditional gas–grain model

Although we are able to model the desorption characteristics of submonolayer mixtures, none of the astrophysical codes currently in use apply Fermi–Dirac statistics or a binding site distribution when simulating the solid–gas exchange. Therefore, we also provide a set of effective binding energies that can be used to simulate the surface segregation/competition of the adsorbates in specific, astrophysically relevant situations. It is possible for us to calculate the desorption flux for any initial population on the surface, at any temperature, using equation (9). It is therefore possible to compare this ϕ_{out} to the classical desorption rate of equation (1) and to derive the effective binding energy, $E_{b,eff}$, that would give the same result. The results of these calculations for various submonolayer mixtures of CO with 0.05 ML O_2 are shown in Table 3.

We have chosen to express the variation of the effective binding energy as a function of CO coverage (and not of O_2 coverage) for

Table 3. Effective binding energy of CO and O$_2$ as a function of CO coverage. These values are calculated assuming a pre-exponential factor $A = 10^{12}$ s^{-1} and have an associated experimental uncertainty of ~ 5 per cent.

N(CO)	0	0.1 ML	0.3 ML	0.8 ML	>1 ML
$E_{b,eff}$(CO)	–	1300	1180	970	863
$E_{b,eff}$(O$_2$)(0.05 ML)	1290	1210	1120	920	912

two reasons. The first one has a physical basis: it is primarily the CO coverage that physically dominates the effective binding energy, as we have shown above. The second reason for this choice has an astrophysical origin: CO abundances are significantly greater than those of O$_2$ in the gas phase. The only O$_2$ detections in the gas phase show maximum abundances of a few 10^{-6} with respect to n_{H_2} in a unique, relatively hot region (Goldsmith et al. 2011), and a few 10^{-8} in a colder region, whereas CO is usually observed at abundances of around 10^{-4}. It is therefore reasonable to assume that CO should also be more abundant than O$_2$ in the solid phase.

It is probable that O$_2$ is formed chemically on the surface of dust grains by the addition of 2 O atoms from the gas phase. The gas phase density of O is mostly unknown, but is usually assumed in models to be about equal to the CO abundance. Therefore, the rather high solid state diffusion rate of O (Congiu et al. 2014) should lead to the formation of O$_2$, which will remain on the dust grain surface as soon as some water ice coats the substrate ($A_v > 3$; Whittet et al. 1988) to prevent any possible chemical desorption (Minissale & Dulieu 2014). However, as soon as CO is present on the surface, CO$_2$ formation by O addition becomes efficient (Minissale et al. 2013), in addition to other competitive mechanisms deriving from H addition to O and O$_2$, such as the formation of H$_2$O (Dulieu et al. 2010; Miyauchi et al. 2008). Therefore a scenario involving accumulation of O$_2$ in the solid phase seems unrealistic. Conversely, evidence of solid CO has been widely established (Whittet & Duley 1991; Tielens et al. 1991). This is the main reason why we provide the variation of the binding energy only as a function of the CO coverage in Table 3.

The value of 0.05 ML of O$_2$ was chosen as being representative of a trace amount of the molecule present on the grain, while simultaneously corresponding to a reasonable experimental accuracy. The binding energies calculated using the Fermi–Dirac distribution approach are therefore not based on a blind extrapolation of experimental data. With higher O$_2$ coverages, the binding energy values will reduce a little, as is seen for CO (second row, Table 3). However, higher coverages are unlikely in an astrophysical context.

The effect of submonolayer CO coverage on the binding energy has already been demonstrated (Noble et al. 2012), and our current values show a very satisfactory agreement with our previous results: 1307 K for 0.1 ML (Noble et al. 2012), compared with 1300 K calculated here, a result which is well within the experimental uncertainty of ~ 5 per cent. With an increase in coverage, the effective binding energy tends towards the multilayer value that is unchanged from the previous study.

One completely new result revealed by the current study is that the evolution of the binding energy of very low (~ 0.05 ML) coverages of O$_2$ is highly dependent on the presence of CO adsorbed on the surface. We can, in fact, quantify the dislodging effect that CO exerts on O$_2$. The effective binding energy of 0.05 ML of O$_2$ on a grain is 1290 K. The addition of only 0.1 ML of CO reduces the O$_2$ binding energy by 80 K (about 8 per cent), corresponding to about a quarter of the total variation in the binding energy of O$_2$ (368 K). This numerical proof of the dislodging of O$_2$ by CO illustrates the

potential importance of this mechanism to the physicochemistry of O$_2$ on grains.

5 ASTROPHYSICAL IMPLICATIONS

5.1 Astrophysical quantities

When considering the desorption process on an astrophysical scale, the desorption flux must be compared to the accretion flux, which can be written as

$$\phi_{in} = \frac{1}{4}nv,$$

where n is the density of the molecule, and v the average speed in the gas phase. For a hypothetical 'standard' cloud, where the grain temperature, T_s, and the gas temperature, T_g, are equilibrated and equal to 10 K, with a density of particles of 10^4 cm^{-3} and a CO density of 1 cm^{-3}, the accretion flux is around 70×10^2 mol cm^{-2} s^{-1}.

It is important to note that accretion is above all (but not only) dependent on the density of molecules and, consequently, on the density of the cloud. In the examples below, we will assume a CO density of around 10^{-4} relative to H$_2$ which is a standard value used in models. The case of O$_2$ is more problematic, since many models predict a much larger abundance of this molecule than that which is observed. We will use 10^{-6} (Goldsmith et al. 2011), the highest value ever observed, keeping in mind that this observation was made towards a hot region where physical conditions are far from the hypothetical 'standard' cloud we are discussing. The value of around 10^{-8} (Larsson et al. 2007) was observed in a region corresponding much more to the conditions we are exploring, however, we have decided use the highest value as an upper limit on gas phase O$_2$ and thus make upper limit predictions for O$_2$ using our experimental desorption data.

To determine whether depletion from the gas phase may occur, one must first compare the incoming flux, ϕ_{in}, to the outgoing flux, ϕ_{out}. The area of the surface, linked to the size distribution of grains, does not matter because the accretion surface is equivalent to the desorption surface. However, this solid surface is very important when calculating the freeze-out time-scale. Such a consideration does not fall within the scope of the current article and we will not detail this aspect here, instead making the assumption that the accretion time on grains is always larger than the free-fall time. We can consider that $T_s = T_g = T$ because, as we ignore all other desorption processes such as photodesorption, our study is only relevant to dark clouds where gas and grain temperatures are equilibrated. As previously mentioned, the density of the cloud is a key parameter for accretion, but the most sensitive parameter remains the temperature of the grains, since the desorption has an exponential dependence on it. The variation in the desorption overcomes the small variation in the accretion due to the change of the speed of molecules in the gas phase.

It is important to highlight the fact that there are two ways to achieve depletion in the gas phase: the first one consists of accumulating CO (or O$_2$) as multilayers, which only depends on the ratio between CO adsorption and CO desorption; the second possibility consists of accreting CO on the surface, from which it disappears chemically, for example by O, H, or OH addition. In the second scenario, the incoming flux, diffusion, and reactivity will play a role. We do not include this scenario here, not because it is irrelevant, but instead because diffusion and surface chemistry are outwith the scope of our current experimental study. This subject will have to
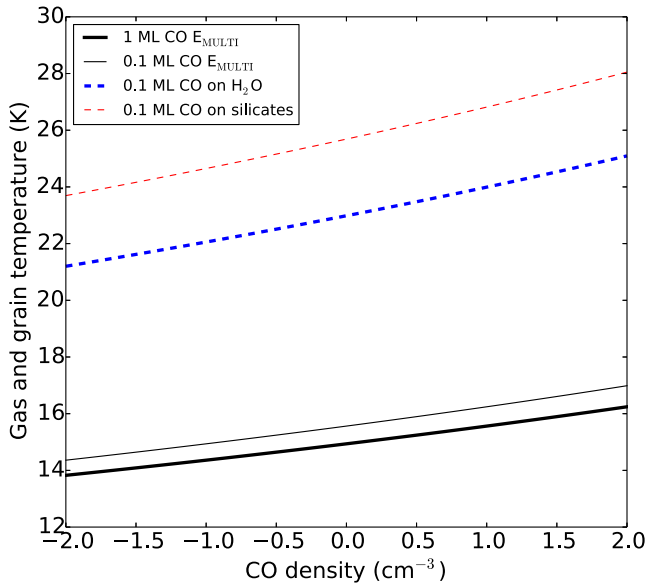
Figure 7. CO freeze-out border line. The *x*-axis is the CO density on a log scale, while the *y*-axis is the gas and grain temperature in Kelvin. The equilibrium between adsorption and desorption of molecules occurs along the plotted lines, with the traditional depletion regime (more than 1 ML can be absorbed, based on the multilayer desorption energy) at temperatures below the thick black line. The thin black line represents 0.1 ML of adsorbed molecules with a constant *E*. The thick red and blue lines represent the situation where 0.1 ML of CO is adsorbed on bare grains and water coated grains, respectively, with a distribution of binding energies.

be treated carefully with a complex simulation. In this work, we discuss only the case of CO (and O_2) adsorbed on dust grains, not considering its fate after accretion. It is commonly agreed that ice mantles are composed of (up to) several hundred layers and that, depending on the medium, about 10–30 per cent of the total mantle is CO (e.g. Whittet et al. 1988; Tielens et al. 1991; Pontoppidan et al. 2003). In either depletion scenario – simple accumulation or complex solid state chemistry – the initial accretion step is highly relevant.

5.2 CO on grains

As we have shown experimentally, CO adsorption is very weakly affected by the presence of O_2, so we first address the question of pure CO adsorption. Our goal is to investigate when and where $\phi_{in}(n, T_g) = \phi_{out}(N, E(N), T_s)$, the condition which defines the equilibrium solid–gas line. At temperatures above this equilibrium line, desorption dominates, while below, accretion will dominate. However, as we will show, the equilibrium is highly dependent on the surface coverage, and so can dynamically change with any changes in the coverage. The surface density parameter, *N*, is very important since it has a large effect on *E*, but it is a puzzling parameter because it correlates the outgoing flux to the incoming flux. Starting with a bare surface, the outgoing flux is strictly null, but as soon as one molecule lands, the desorption flux rises and the desorption does not only rise linearly with *N*, as previously believed, but much more efficiently thanks to the decrease of the binding energy. With the increase of the coverage, the desorption flux rises very rapidly and balances the accretion, and a steady state, the specific surface density that equilibrates adsorption and desorption, appears.

In Fig. 7, the condition $\phi_{in} = \phi_{out}$, is plotted on a diagram of temperature versus gas phase CO density. The thick black line rep-

resents the thermal freeze-out equilibrium, because it is calculated using the multilayer binding energy of CO at the maximum surface coverage of 1 ML. If more CO accumulates in the solid phase, the surface coverage does not increase (the bulk coverage does), and consequently the binding energy of CO does not vary because it is already at its minimum. Thus, the desorption rate cannot increase any more (for a given temperature). Below this limit, the accretion into the solid phase is not compensated for by an increase in desorption and, therefore, molecules will certainly accumulate in the solid phase.

By assuming that the CO binding energy is equivalent to a single value (the multilayer binding energy) we determine the limit of depletion from the gas phase, i.e. the line below which depletion certainly occurs (Fig. 7, thick black line). Calculated in this way, the CO freeze-out line is independent of the nature of the substrate, and lies in the 14–16 K range for typical CO densities (10^{-2}–10^2, corresponding to clouds with densities of 10^2–10^6). The thin black line in Fig. 7 corresponds to 0.1 ML of adsorbed CO, using the traditional, commonly used assumption that the binding energy for each molecule is the same unique multilayer value. The line is shifted by about 1 K in comparison with the 1 ML (and more) coverage (thick black line). This corresponds to the fact that the desorbing flux is reduced by the surface density, which is ten times lower than the full coverage. To compensate for this partial coverage, the surface temperature has to be slightly higher in order to balance the accretion flux. We point out here that if the surface coverage increases, the desorbing flux proportionally increases. On the thin black line, depletion from the gas phase cannot occur, because if more molecules accrete, the desorbing flux increases, and no accumulation can occur except if the temperature decreases to compensate the coverage-dependent desorption. Between the thin black line and the thick black line fall all of the coverages from 0.1–1 ML. Except in cases where there is a fast chemical transformation of CO, gas phase depletion is not expected. We can see that both black lines are very close in temperature, and that partial accretion on the solid surface (thin line) and certain depletion from the gas phase (thick line) are almost merged.

However, we know that this single energy approach is outdated, and that a surface-density-dependent desorption energy must be used. The blue and red lines correspond to the situation where 0.1 ML of adsorbate is present on the surface, taking into account the variation of binding energies with the coverage; the blue line corresponds to water-coated grains and the red line to bare silicate surfaces. The temperature is more than 20 K for both and is about 2 K higher for bare grains than for icy grains. These lines correspond to conditions where, if depletion from the gas phase is not possible by simple adsorption, chemical activity on grains is certain, because this line corresponds to the equilibrium 0.1 ML of adsorbate.

5.3 O_2 on grains in presence of CO

Fig. 8 illustrates how the surface coverage of adsorbates at the equilibrium condition $\phi_{in} = \phi_{out}$ varies with temperature for a cloud of $n = 10^4$ cm^{-3}, with an O_2 gas phase upper abundance of 10^{-6} and a standard CO abundance value of 10^{-4}. We have plotted the results for temperatures between 10 and 30 K, relevant for dark molecular clouds. The dotted line denotes 17 K, the temperature above which the surface coverage decreases from a full monolayer coverage; this is also the regime in which our model's assumptions are valid, and where it provides new insights. For CO (red line), the 0.1 ML line is crossed at around 23 K, coherent with Fig. 7. We notice that even at a relatively high temperature (30 K) the surface
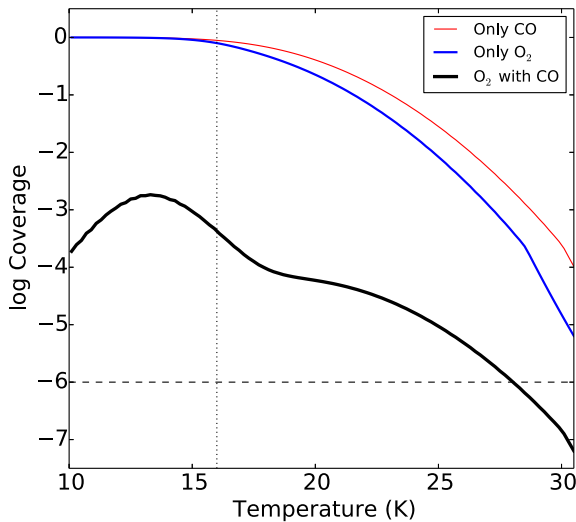
Figure 8. Surface coverage of CO and O_2 as function of temperature at the surface of grains in a cloud of $n(CO) = 1$ and $n(O_2) = 10^{-2}$ cm^{-3}. The blue line (O_2 coverage) corresponds to the surface density calculated without competition with CO, and the black line includes the dislodging mechanism. The dashed line represents a surface coverage of one molecule for our standard grain, and is therefore considered as a lower limit. The dotted line represents the thermal equilibrium.

coverage of CO is about 10^{-4}, which represents 100 molecules per grain, assuming a spherical grain of average radius 0.1 micron, and therefore $\sim 10^6$ adsorption sites on its surface. If competition for adsorption sites on the icy grain surface were not taken into account, we would expect approximately the same behaviour in the case of O_2 (blue line). However, when we include the segregation mechanism presented above, the surface density of O_2 is reduced by 2–4 orders of magnitude (black line). The total fraction of O_2 molecules on the surface of dust grains never exceeds 10^{-4} if CO is co-adsorbed; this value is an upper limit which takes into account the very optimistic gas phase density of O_2 used in our example. The very low value of O_2 surface coverage found at this point further validates the choice we made when compiling Table 3, i.e. we provided effective binding energies for 0.05 ML O_2 co-adsorbed with CO. Lower coverage values would lead to minor variations in the energies, but at such low coverages these variations are very sensitive to the exact shape of the binding energy distribution that we used.

From the data presented in Figs 7 and 8, we can conclude that CO and O_2 have different fates during the adsorption process on grains. Below ~ 15 K, the accretion of both CO and O_2 can proceed without any influence from the segregation mechanism, and thus there will be no selectivity in the depletion. Below this temperature, depletion from the gas phase is certain if other mechanisms cannot balance the freeze-out. Assuming thermal equilibrium, we can conclude that surface segregation and competition expel most of the O_2 from the surface for temperatures above 17 K. CO, on the other hand, is at least partly adsorbed on the surface of dust grains at typical temperatures of less than 23.5 K for one tenth of a monolayer surface coverages, and 30 K for a few CO molecules. These temperatures are significantly higher than the depletion limit calculated when assuming a multilayer binding energy. Thus, the segregation effect imposes a selectivity in the potential for these two species to deplete. The depletion of O_2 is limited for surface temperatures above 17 K due to the presence of CO, which will be present on surfaces in trace quantities at grain temperatures below 30 K. At the higher temperatures considered here (17–30 K) the role of the grains is very important, but depletion from the gas phase may still be possible if the accretion of the molecular species is followed by a chemical transformation. However, at these temperatures, CO should force O_2 back into the gas phase, and therefore, if O_2 is not chemically consumed, surface segregation could be one of the mechanisms responsible for the few observations of O_2 that have been made.

6 CONCLUSION AND PERSPECTIVES

Contrary to what happens in the multilayer regime, O_2 and CO co-adsorbed on an amorphous surface show very different desorption behaviour when mixed than when adsorbed separately. CO molecules dislodge O_2 molecules thanks to a slightly higher affinity with the surface. Although the binding energy distribution, centred at 1100 K, is only shifted by 85 K, this small difference is enough to provoke a strong reduction of the binding energy of O_2 in the presence of CO. It is possible to model this behaviour with a distribution of the adsorbates in the different available binding sites defined using the Fermi–Dirac statistical repartition law. Based on this model, we have proposed effective binding energy values for different CO coverages, assuming a trace amount of O_2 co-adsorbed on dust grains. The surface segregation mechanism should not change the depletion mechanism for dust temperatures lower than 15 K. However, it appears that there is a wide range of temperatures (15–30 K) where dust grains will be covered with a fraction of a layer of CO and where solid-state chemistry will occur. O_2 present on the grain, on the other hand, will be forced to thermally desorb in this temperature range.

The presence of O_2 in the gas phase has only been observed in three regions, under specific physical conditions (Larsson et al. 2007; Goldsmith et al. 2011; Yıldız et al. 2013). The dislodging mechanism induced by surface segregation could play a role in its return to the gas phase. In order to quantify this aspect, however, it will be necessary to use a dedicated model including solid state chemistry. In fact, desorption fluxes, needed to balance the accretion flux, have to be compared to the accretion fluxes of others plausible reactants, such as H and O. If the reactivity of O_2 on the grain is faster than the forced desorption, then it cannot be the source of observed O_2.

More generally, the surface segregation mechanism is likely to occur as soon as molecules with similar properties are present on an amorphous surface. We have shown that this is true in the case of O_2 and CO, but it is also probably the case for N_2, which will be the subject of our next study. It is probable that similar microscopic behaviours will be found, but in order to be the most applicable to astrophysics, i.e. for those species that selectively deplete from the gas phase, it would be useful to include dynamical studies of the effect. In real molecular clouds, the density and the temperature are continually and simultaneously evolving, and it is possible that the dislodging mechanism, although it seems to be relatively inefficient in the steady state conditions used here, can make a large difference to the gas and solid phase abundances of key species.

REFERENCES

Acharyya K., Fuchs G. W., Fraser H. J., van Dishoeck E. F., Linnartz H., 2007, A&A, 466, 1005

Amiaud et al., 2015, Phys. Phem. Phem. Phys., submitted

Amiaud L., Fillion J. H., Baouche S., Dulieu F., Momeni A., Lemaire J. L., 2006, J. Chem. Phys., 124, 094702

Amiaud L., Momeni A., Dulieu F., Fillion J. H., Matar E., Lemaire J.-L., 2008, Phys. Rev. Lett., 100, 056101

Bacmann A., Lefloch B., Ceccarelli C., Castets A., Steinacker J., Loinard L., 2002, A&A, 389, L6

Bacmann A., Taquet V., Faure A., Kahane C., Ceccarelli C., 2012, A&A, 541, LL12

Bergin E. A., Tafalla M., 2007, ARA&A, 45, 339

Bertin M. et al., 2013, ApJ, 779, 120

Bisschop S. E., Fraser H. J., Öberg K. I., van Dishoeck E. F., Schlemmer S., 2006, A&A, 449, 1297

Bossa J.-B. et al., 2014, A&A, 561, AA136

Burke D. J., Brown W. A., 2010, Phys. Chem. Chem. Phys., 12, 5947

Caselli P., Walmsley C. M., Tafalla M., Dore L., Myers P. C., 1999, ApJ, 523, L165

Chaabouni H. et al., 2012, J. Chem. Phys., 137, 234706

Chiar J. E., Adamson A. J., Kerr T. H., Whittet D. C. B., 1995, ApJ, 455, 234

Collings M. P., Frankland V. L., Lasne J., Marchione D., Rosu-Finsen A., McCoustra M. R. S., 2015, MNRAS, 449, 1826

Congiu E., Chaabouni H., Laffon C., Parent P., Baouche S., Dulieu F., 2012, J. Chem. Phys., 137, 054713

Congiu E. et al., 2014, Faraday Discussions, 168, 151

Dohnalek Z., Kimmel G. A., Joyce S. A., Ayotte P., Smith R. S., Kay B. D., 2001, J. Phys. Chem. B, 105, 3747

Dulieu F., Amiaud L., Baouche S., Momeni A., Fillion J.-H., Lemaire J. L., 2005, Chem. Phys. Lett., 404, 187

Dulieu F., Amiaud L., Congiu E., Fillion J.-H., Matar E., Momeni A., Pirronello V., Lemaire J. L., 2010, A&A, 512, AA30

Dulieu F., Congiu E., Noble J., Baouche S., Chaabouni H., Moudens A., Minissale M., Cazaux S., 2013, Sci. Rep., 3, 1338

Fayolle E. C., Öberg K. I., Cuppen H. M., Visser R., Linnartz H., 2011, A&A, 529, AA74

Goldsmith P. F. et al., 2011, ApJ, 737, 96

Hama T., Watanabe N., 2013, Chem. Rev., 113, 8783

Honvault P., Jorfi M., González-Lezana T., Faure A., Pagani L., 2011, Phys. Rev. Lett., 107, 023201

Kimmel G. A., Stevenson K. P., Dohnálek Z., Smith R. S., Kay B. D., 2001, J. Chem. Phys., 114, 5284

Kristensen L. E., Amiaud L., Fillion J.-H., Dulieu F., Lemaire J.-L., 2011, A&A, 527, AA44

Larsson B. et al., 2007, A&A, 466, 999

Lis D. C., Bergin E. A., Schilke P., van Dishoeck E. F., 2013, J. Phys. Chem. A, 117, 9661

Minissale M., Dulieu F., 2014, J. Chem. Phys., 141, 014304

Minissale M., Congiu E., Manicò G., Pirronello V., Dulieu F., 2013, A&A, 559, A49

Minissale M., Congiu E., Dulieu F., 2014, J. Chem. Phys., 140, 074705

Miyauchi N., Hidaka H., Chigai T., Nagaoka A., Watanabe N., Kouchi A., 2008, Chem. Phys. Lett., 456, 27

Noble J. A., Dulieu F., Congiu E., Fraser H. J., 2011, ApJ, 735, 121

Noble J. A., Congiu E., Dulieu F., Fraser H. J., 2012, MNRAS, 421, 768

Öberg K. I., van Dishoeck E. F., Linnartz H., 2009, A&A, 496, 281

Pagani L., Bacmann A., Cabrit S., Vastel C., 2007, A&A, 467, 179

Pagani L., Bourgoin A., Lique F., 2012, A&A, 548, LL4

Pontoppidan K. M. et al., 2003, A&A, 408, 981

Tielens A. G. G. M., Tokunaga A. T., Geballe T. R., Baas F., 1991, ApJ, 381, 181

Whittet D. C. B., Duley W. W., 1991, A&AR, 2, 167

Whittet D. C. B., Bode M. F., Longmore A. J., Adamson A. J., McFadzean A. D., Aitken D. K., Roche P. F., 1988, MNRAS, 233, 321

Willacy K., Millar T. J., 1998, MNRAS, 298, 562

Yıldız U. A. et al., 2013, A&A, 558, AA58

This paper has been typeset from a TEX/LATEX file prepared by the author.